Wave drag by three-dimensional mountain lee-waves in nonplanar shear flow

By WILLIAM BLUMEN and CARY D. McGREGOR, *Department of Astro-Geophysics, University of Colorado, Boulder, Colorado 80309, USA*

(Manuscript received June 30; in final form December 9, 1975)

ABSTRACT

The effect of both cross-wind and vertical shear of the basic flow are considered in a linear, hydrostatic model of stationary, mountain lee-waves in a stably stratified airstream. Analytical solutions are first determined for a constant lapse rate basic-state. A solution corresponding to a cross-wind variation, represented by the hyperbolic secant profile, is compared with a constant flow over the same isolated hill. In the former case, wave-energy is trapped by the background shear. This effect is responsible for a greater wave-drag on the airstream than the drag produced in the constant wind case. However, these values of the wave-drag are always less than the drag exerted by two-dimensional waves over a ridge. A two-layer model is then considered, in order to examine the effect of a stable stratosphere over a less stable troposphere. The results show that the drag is sensitive to the phase difference between the transmitted and reflected waves in the lower layer. This sensitivity is more pronounced when cross-stream shear of the basic flow is taken into account. Finally, the relationship between the present model dynamics and the mechanism suggested for the dynamics of wave-induced downslope winds, presented by Klemp & Lilly, is pointed out.

1. Introduction

It is known that mountain lee-waves can transport momentum from a stably stratified airstream to the earth's surface in response to a net pressure drop between the windward and lee slopes of an isolated mountain or ridge. Sawyer (1959) first pointed out the relative importance of this momentum loss, due to wave drag by small-scale stationary lee-waves (horizontal wave length $L \sim 10$–100 km), in comparison with surface frictional drag over rough terrain. Sawyer examined a case of two-dimensional flow over a bell-shaped obstacle and determined that the typical surface stress is order 1–10 dynes cm^{-2}. Sawyer's estimate of the surface stress was later confirmed by Blumen (1965), who considered randomly distributed orography, three-dimensional effects and a two-layer representation of the thermal stratification and basic wind shear. Bretherton (1969) provided additional confirmation by computing the stress due to two-dimensional flow over the Welsh mountains using observed atmospheric conditions. A conclusive verification of the importance of lee-wave drag, at least over the Front Range of the Colorado Rockies, was obtained from data collected by instrumental aircraft and reported by Lilly (1972): "From aircraft traverses through moderate amplitude waves in the Front Range we have commonly obtained direct stress measurements of between 5 and 10 dynes cm^{-2} in the troposphere, averaged over a horizontal distance of 100–200 km."

While research during the past sixteen years has established that momentum flux by lee waves, and other meso-scale phenomena, is an important subgrid-scale physical feature, its effect on large-scale dynamical processes has not yet been explicitly incorporated into prediction or general circulation models. Away from critical levels, linear theory does not provide information concerning the levels at which the wave drag acts: without dissipation the stress divergence is identically zero. Observations over the Colorado Rockies, while not conclusive, suggest that the momentum loss is most pronounced at stratospheric levels where wave breakdown into turbulence occurs. However, this latter effect is difficult to incorporate, by parameterization, into large-scale numerical models.

The observations noted above appear to indicate that linear lee-wave theory will provide useful information on area-averaged stress in the troposphere for the development of viable parameterization schemes. Linear theory cannot be expected to provide detailed information on the structure of large-amplitude waves, as noted recently by Smith (1976). However, observational verification of a linear theory developed by Klemp & Lilly (1975), for the dynamics of strong downslope winds associated with lee-waves above the Colorado Rockies, has been sufficiently encouraging to suggest use of their model for operational forecasting purposes.

A critical feature in the evaluation of wave drag, as well as in the windstorms described by the Klemp–Lilly model, is the vertical structure of the basic wind and temperature distribution. Blumen (1965) has shown that the magnitude of the wave drag is very sensitive to the vertical wavelength L_z; a maximum value is attained when the tropopause height H_0 is one-half L_z. The vertical wavelength of the standing lee-wave is determined by the horizontal wavelength, the static stability, measured by the Brunt-Väisälä frequency, and the vertical wind-profile. Correspondingly, the calculations of lee-wave drag will depend on how well numerical models depict vertical atmospheric structure. The sensitivity of the drag to vertical structure is directly related to the transmission of wave energy from mountain level to upper levels, where selective reflection and refraction occur. The amount of energy that can reach stratospheric levels, where the principal momentum losses are expected to occur, must be accurately determined in any parameterization of this phenomenon. Consequently, the relative importance of all features that can affect this process must be evaluated. The purpose of the present study is to evaluate the effect of cross-wind variation of the basic flow on wave momentum-flux. This feature of the basic flow has not previously been included in any lee-wave model known to the authors. However, as we point out in section 3, the present results have been obtained with a model in which the scale of the wind shear is the same as that of the hill. Consequently, some of the specific results would be modified by more general flows, although some general features of the wave response in the presence of cross-stream shear should be well represented by the present model. Our results show that significant values of lateral shear will cause an appreciable change in the vertical wavelength of the stationary lee-wave pattern which, in turn, will affect the relationship between the wave-drag and tropopause height in the two-layer model employed in this study. By analogy, lateral shear may be expected to affect predictions of downslope windstorms, in some cases, since the vertical wavelength is also a critical parameter in the Klemp–Lilly model.

The three-dimensional model is presented in section 2. A solution for flow over an isolated obstacle is displayed in section 3, for purposes of isolating the principal effect of cross-stream variation of the basic flow. Drag coefficients for two- and three-dimensional flow of a constant lapse rate atmosphere are compared in section 4. In section 5, the wave solutions for a two-layer model are presented and used to evaluate the mutual effects of both a stratospheric layer of high static stability and lateral shear in both layers on the drag coefficient. Some concluding remarks appear in section 6.

2. Model

The model employed in the present work has been used to study neutral and unstable waves by Blumen (1971*a*, 1975), when the fluid was assumed bounded from above and below by level surfaces upon which the vertical velocity identically vanishes. Before modifying the boundary conditions, for present purposes, the model assumptions will be displayed. These assumptions are:

1) steady-state flow;
2) inviscid flow;
3) earth's rotation neglected;
4) Boussinesq approximation;
5) linear perturbation theory, and;
6) both the basic-state *and* perturbations satisfy hydrostatic balance.

A discussion of these assumptions will be presented after the appropriate nondimensional parameters and boundary conditions have been introduced.

The velocity scale U denotes the characteristic amplitude of the basic zonal flow; the length scales L and H are characteristic horizontal and vertical dimensions, which will be specified below. In a Cartesian frame, x^* and y^* are directed to the east and north respectively, z^* is directed upward, antiparallel to gravity g. The basic flow $\bar{u}^*(y^*, z^*)$ is directed along the x^*-axis and the velocity perturbations (u^*, v^*, w^*) are (x^*, y^*, z^*) directed. Pressure and density are denoted by p^* and ϱ^*. The nondimensional variables, used hereafter, are defined as

$$(x, y) = (x^*, y^*)/L, \quad z = z^*/H,$$
$$(\bar{u}, u, v, Hw/L) = (\bar{u}^*, u^*, v^*, w^*)/U,$$
$$\pi = p^*/\bar{\varrho}^* U^2 \tag{1}$$

Note that in anticipation of employing the hydrostatic approximation for the perturbation flow, the vertical velocity has been scaled by the factor H/L in addition to U. The appropriate lower boundary condition is

$$w^*(x^*, y^*, h^*) = (\bar{u}^* + u^*)h^*_{x^*} + v^* h^*_{y^*} \tag{2}$$

where $h^*(x, y) = ah(x, y)$ is the mountain profile characterized by amplitude a and form $h(x, y)$. In nondimensional form,

$$w(x, y, ah/L) = \varepsilon[(\bar{u} + u)h_x + vh_y] \tag{3}$$

where $\varepsilon = a/H \ll 1$ and $H \sim 8$ km, typical of an atmospheric scale-height. We shall further assume that

$$\delta^2 = (H/L)^2 \ll 1 \tag{4}$$

where δ denotes the aspect ratio. The characteristic values of ε and δ permit linearization of the boundary condition and, subsequently, the differential equation. Thus (3) becomes

$$w(x, y, 0) = \bar{u}(y, 0)h_x \tag{5}$$

where (u, v, w) are of order ε compared with the basic flow $\bar{u}$. The characteristic horizontal length scale of the lower boundary is, in view of (4), $L \sim 25$ km.

The wave solutions in the present model may be represented in terms of upward and downward propagating components, as expressed by (20), for example. In the uppermost layer of our model atmosphere only the upward propagating Fourier components, for which

$$\overline{\pi w} > 0 \tag{6}$$

will be retained, where the bar denotes an average over one wavelength in the x-direction. This condition (6), introduced by Eliassen & Palm (1961), has also been applied by Klemp & Lilly (1975) in their treatment of long waves, i.e., horizontal wavelengths $L_x > H$.

It is now appropriate to summarize the basic assumptions. Only inviscid, steady-state solutions will be considered. The basic flow (13), used in this study, is *not* unstable to stationary disturbances ($\partial/\partial t \equiv 0$). However, Blumen (1971*b*) has shown that inflection-point instability to long travelling waves occurs. The e-folding time for the characteristic wavelengths of the present model is about 5–6 h. This value is comparable with the characteristic time during which a stationary lee-wave pattern becomes established (Foldvik & Wurtele, 1967). Consequently, there is some doubt raised about the steady-state assumption employed here. Moreover, this question could also be raised about the validity of other lee-wave studies as well, since the assumption that the basic flow remains steady for periods greater than 5–6 h, even in the absence of inertial instabilities, is not well-founded. However, the unstable growth rates have been determined from a model of homogeneous shear flow. The existence of stable stratification could be expected to reduce the growth rates because some of the energy gained from the basic flow would be used to do work against buoyancy.

The effect on the wave solutions due to the earth's rotation will be neglected because the Rossby number, $R_0 = U/f_0L$, is typically order 10 for $U \sim 20$ m sec^{-1}, $L \sim 25$ km and a Coriolis parameter $f_0 \sim 10^{-4}$ sec^{-1}. The Boussinesq approximation is employed, since we are essentially interested in surface stress. However, the wave solutions should be modified by multiplying the perturbation velocity and density fields by $\bar{\varrho}(z)^{\frac{1}{2}}$ and the π field by $\bar{\varrho}(z)^{-\frac{1}{2}}$ for an approximate description at higher levels. This procedure will not be carried out to retain simplicity in the analysis. The linearization rests upon the assumption that the orography is of small-amplitude ($a/H \ll 1$) and limited in slope ($H < L$). The hydrostatic approximation follows from the restriction placed on the aspect ratio in (4). This assumption is not always appropriate in pronounced lee-wave situations, where vertical accelerations may not be negligible. However, the relatively good agreement between observations and theory, reported by Klemp & Lilly, was used to support the use of the hydrostatic approximation for the scales of motion examined in the present study.

Under the above assumptions, Blumen (1975) has shown that the wave equation governing the pressure perturbation amplitude $\hat{\pi}(y, z)$ is given by

$$(\bar{u}^{-2}\hat{\pi}_y)_y - \alpha^2\{\bar{u}^{-2}\hat{\pi} + (J^{-1}\hat{\pi}_z)_z\} = 0 \tag{7}$$

where α denotes the x-wave number and the complete solution $\pi(x, y, z)$ is represented by a Fourier integral over all values of α (see section 3); the parameter $J(z)$ may be interpreted as a static stability measure, so that for an incompressible fluid,

$$J(z) = (-gd \ln \varrho^*/dz^* H^2)/U^2 \tag{8}$$

In a compressible medium, density is replaced by potential density.

The wave eq. (7) has a desirable analytical property that will be exploited. If the basic flow is represented in the separable form

$$\bar{u}(y, z) = F(y)G(z) \tag{9}$$

then the pressure amplitude may be determined as a separable solution of (7),

$$\hat{\pi}(y, z) = \Pi(y)P(z) \tag{10}$$

The separated equations governing the pressure amplitude in (10) are

$$G^2[P'' - (J'/J)P'] + J(\lambda^2/\alpha^2)P = 0 \tag{11}$$

$$F\Pi'' - 2F'\Pi' - \alpha^2 F[1 - (\lambda^2/\alpha^2)F^2]\Pi = 0 \tag{12}$$

where λ^2 is the separation constant and J is defined by (8). Particular solutions of (11) and (12), satisfying the boundary conditions (5) and (6) will be considered in sections 3 and 5.

3. One-layer atmosphere

(a) basic state

A principal effect of cross-stream variation of the wind profile can be isolated by considering an atmosphere of infinite vertical extent with a basic flow independent of height. Since the general solution of (12) has not been obtained, attention will be restricted to a particular solution. For the present case, J is treated as a constant, $J = J_0$. Although this model is now formally equivalent to an isothermal model atmosphere, we shall consider the analysis as applying to an atmosphere that has a uniform lapse rate that is not necessarily isothermal.

The basic flow is represented by

$$\bar{u}(y) = \operatorname{sech} y \tag{13}$$

(b) Wave solution

The relationship between the amplitudes of the vertical velocity and pressure perturbation may be determined from the thermodynamic energy and hydrostatic equations presented by Blumen (1975, eqs. (4) and (6)). This relationship is

$$\hat{w}(y, z) = -i\alpha J^{-1}\bar{u}[\hat{\pi}(y, z)]_z \tag{14}$$

where $\hat{\pi}$ is represented by (10). A particular solution of (12) is given by

$$\Pi(y) = \operatorname{sech}^\gamma y \tag{15}$$

where

$$\gamma = 1 + (1 + \alpha^2)^{\frac{1}{2}} \tag{16}$$

while the separation constant in (11) and (12) satisfies

$$\lambda^2 = (1 + \alpha^2)^{\frac{1}{2}}[1 + (1 + \alpha^2)^{\frac{1}{2}}] \tag{17}$$

Introduction of (13) and (15) into (14) yields

$$\hat{w}(y, z) = -i\alpha J_0^{-1} \operatorname{sech}^{\gamma+1} y P_z \tag{18}$$

where J_0 is the constant value of J. Moreover, introduction of (18) into (11) determines the z-amplitude equation for the vertical velocity perturbation,

$$W'' + [(\lambda/\alpha)^2 J_0 G^{-2} - G''G^{-1}]W = 0 \tag{19}$$

where $G(z)$ is given by (9) and λ^2 by (17). Since the basic flow is independent of height in this case, we set $G \equiv 1$. In general, (19) is the hydrostatic counterpart of the wave equation used in most studies of two-dimensional flow over a ridge. The term in brackets is the so-called Scorer parameter for the present model.

From (18) and (19), we obtain the vertical velocity amplitude

$$\hat{w}(y, z) = \operatorname{sech}^{\gamma+1} y[A_1(\alpha)e^{imz} + A_2(\alpha)e^{-imz}] \quad (20)$$

where

$$m^2 = (\lambda/\alpha)^2 J_0 \quad (21)$$

and the A's are constants, determined by the boundary conditions.

The constant A_2 is set equal to zero to eliminate downward energy flux, as required by condition (6). In order to satisfy the lower boundary condition (5), the ground contours must vary with y like $\Pi(y)$ in (15); the x-variation is arbitrary. We have represented the hill by

$$h(x, y) = \operatorname{sech} yK_0\{[x^2 + (\eta + \ln\cosh y)^2]^{1/2}\}$$
$$= \operatorname{sech} y \int_0^\infty \exp[-(\eta + \ln\cosh y)(1+\alpha^2)^{1/2}]$$
$$\times \frac{\cos\alpha x}{(1+\alpha^2)^{1/2}}\, d\alpha \quad (22)$$

where K_0 denotes the modified Bessel function and η is a constant. We have chosen $\eta = 0.457$ so that $h(0, 0) = 1$. The basic flow and height contours of the hill are shown in Fig. 1. The hill is essentially circular in a planform and bell-shaped in a vertical cross section (see Fig. 3).

As shown in Fig. 1, attention is directed to the particular case when the characteristic half-width of the shear flow is comparable with the characteristic width of the obstacle. As a consequence, the present results will reflect a particular situation in which lateral shear could be expected to produce a significant effect on three-dimensional mountain waves. The question of when this effect would begin to become significant cannot be answered, because the ratio of the width of the shear zone to mountain width could not be varied. Nonetheless, an important advantage is gained from the accessibility of an analytical solution: it can be displayed, and the wave drag computed, with little difficulty. The determination of a more general numerical solution, requiring the use of a three-dimensional grid, would prove costly and more easily subject to error.

Finally, the constant A_1 is determined from (5), (13), and (22). The vertical velocity may then be represented by the Fourier integral

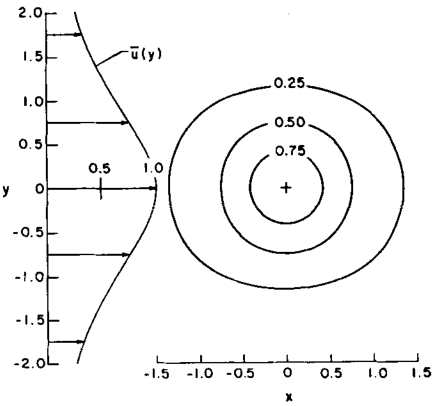

Fig. 1. Basic wind profile $\bar{u}(y)$, represented by (13) and height contours of the hill, given by (22).

$$w(x, y, z) = \operatorname{Re}\, i \operatorname{sech}^2 y \int_0^\infty \frac{\alpha}{(1+\alpha^2)^{1/2}}$$
$$\times \exp[-(\eta + \ln\cosh y)(1+\alpha^2)^{1/2}$$
$$+ i(\alpha x + mz)]\, d\alpha. \quad (23)$$

Eq. (23) was evaluated numerically by means of a Fast Fourier Transform (FFT) program supplied by the Computing Facility of the National Center for Atmospheric Research. These values were compared with the analytically determined value $w(x, y, 0)$, shown in Fig. 2, and with values determined by the method of stationary phase. Vertical velocities to within an accuracy of one percent could be determined. The results are shown in Figs. 3 and 4. A typical

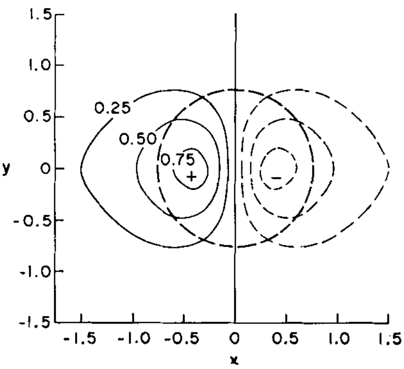

Fig. 2. Vertical velocity field at ground level, $z = 0$. A dimensionless velocity of unity corresponds to $w^* = \varepsilon\delta U \sim (0.71 \times 10^{-1}) \times (0.33) \times 23$ m sec$^{-1} \sim 0.5$ m sec^{-1}. The heavy dashed contour represents the half-width of the hill.

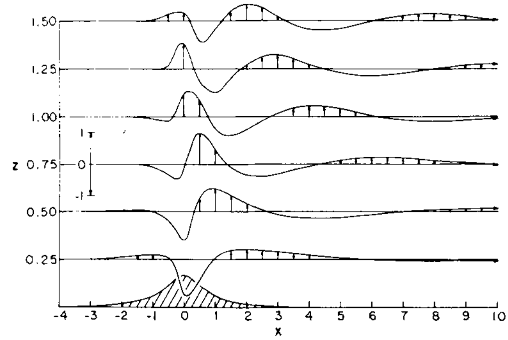

Fig. 3. Cross section of the vertical velocity field at $y = 0$. $\bar{u} = \text{sech}\, y$, $J_0 = 10$, and the vertical velocity scale is given in Fig. 2.

tropospheric value of J_0, measured during lee-wave situations, was used in the evaluation rather than a slightly larger value determined from an isothermal state.

The upstream tilt of the phase lines in Fig. 3 corresponds to upward energy flux, as required by (6). In purely two-dimensional flow over a ridge, no downstream wave appears: the horizontal extent of the wave is limited by the forcing produced by the presence of the obstacle, while the wave propagates freely in the vertical direction transporting energy upward as in Fig. 3. A solution of this latter type was first displayed by Queney (1948). This difference in the two solutions occurs because, in the two-dimensional case, the group and phase velocities are equal, while in the three-dimensional case the x-directed group velocity is less than the phase velocity of the standing wave. Consequently, as the steady-state becomes established in the latter case, wave energy is swept downstream by the basic flow; in the former case wave energy remains near the obstacle.

The vertical velocity determined by a constant

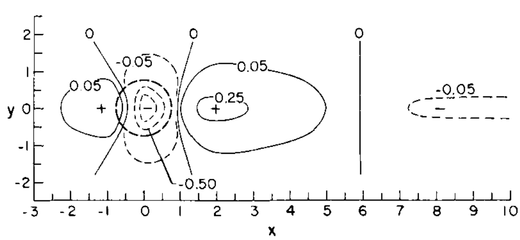

Fig. 4. Vertical velocity field at $z = 0.25$ (2 km). Parameter values are provided in Fig. 3. The heavy dashed contour represents the half-width of the hill.

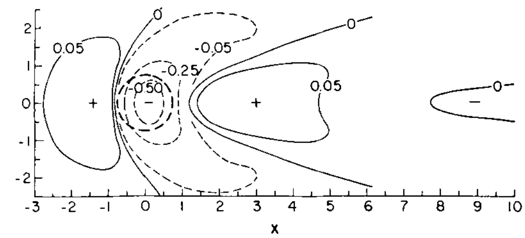

Fig. 5. Vertical velocity field at $z = 0.25$ (2 km). $\bar{u} = 1$, $J_0 = 10$ and the vertical velocity is scaled as in Fig. 2. The heavy dashed curve is as in Fig. 4.

flow of unit amplitude over the hill, given by (22), is displayed in Fig. 5. The wave eq. (7) has constant coefficients and the solution is readily determined to be

$$w(x, y, z) = \text{Re}\; i \int_{-\infty}^{\infty} \int_{0}^{\infty} \frac{\alpha F(\alpha, \beta)}{(1+\alpha^2)^{1/2}} \times \exp\left[-\eta(1+\alpha^2)^{1/2} + i(\alpha x + \beta y + nz)\right] d\alpha\, d\beta \tag{24}$$

where (α, β) are (x, y) wave numbers

$$n^2 = J_0 \frac{\alpha^2 + \beta^2}{\alpha^2} \tag{25}$$

$$F(\alpha, \beta) = \frac{1}{\pi} \int_0^{\infty} \text{sech}^{\gamma}\, y' \cos \beta y'\, dy' \tag{26}$$

and γ is given by (16). $F(\alpha, \beta)$ was determined from Erdélyi et al. (1954, p. 30 (5)) in terms of Gamma functions. The evaluation of (24) was accomplished by means of the FFT program used in conjunction with (23). The results are slightly less accurate due to the more complex numerical evaluations involved.

A comparison of Figs. 4 and 5 shows that downstream from the mountain the phase lines are oriented cross-wind in the former case and obliquely in the latter case. Near the mountain the orientation represents the presence of both the forced and free wave solutions. The flow (13) used to generate the wave solution, displayed in Fig. 4, decays to zero as $|y| \to \infty$. As a consequence a standing wave cannot be maintained as $|y| \to \infty$. In other words, wave energy that is directed cross-wind must be totally reflected; hence, the phase lines of the free waves must lie along the cross-wind direction. In the latter case, where $\bar{u}$ = constant, wave energy propagates cross-wind and is carried downstream during the transient development as the familiar stationary (lee) ship-wave pattern becomes established. Previous investigations, such as Wurtele (1957), have reproduced patterns of the vertical velocity similar to that shown in Fig. 5. Moreover, the existence of lateral shear in the basic flow has a significant effect on the magnitude of the wave drag, which is considered in the following two sections.

4. Wave drag

The downward momentum flux, implied by the upstream tilt of the phase lines in Fig. 3, represents a drag exerted on the atmosphere by the hill. In dimensional units, the drag $D^*(y^*)$ per unit distance in the cross-wind direction is defined as

$$D^*(y^*) \equiv -\bar{\varrho}^* \int_{-\infty}^{\infty} u^* w^* dx^* \tag{27}$$

where $\bar{\varrho}^*$ is the basic-state density at $z^* = 0$, and (u^*, w^*) are perturbation velocities in the (x^*, y^*) directions. It is convenient to express the integral in (27) in dimensionless form by means of (1), in order to define a drag coefficient

$$C_D^* \equiv -(\delta\varepsilon^2 r^*/A^*) \int_{-\infty}^{\infty} uw dx \tag{28}$$

where $A^* = \pi r^{*2}$ is the "effective surface area" occupied by the hill (22) and $r^* = L$ is a radial distance from the center.

The integral in (28) is evaluated in the Appendix for the two cases considered in section 3. $r^*C_D^*$ is displayed in Fig. 6. A comparison of the two cases shows that C_D^* is larger near the origin ($y = 0$) when the basic flow $\bar{u}$ is constant. This circumstance can be explained by examining the individual wave components in each case. The vertical velocities are equal at $y = 0$ because the lower boundary condition (5) is the same in each case. However, the u-components differ. At $y = 0$, $u \propto \pi$ and from (14), the Fourier component is $\hat{u} \propto m^{-1}\hat{w}$, where m is given by (21). In the case of a constant basic flow, $\hat{u} \propto n^{-1}\hat{w}$, where n is given by (25). A comparison of n and m shows that $\beta^2 \geq 0$ in (25) is the counterpart of

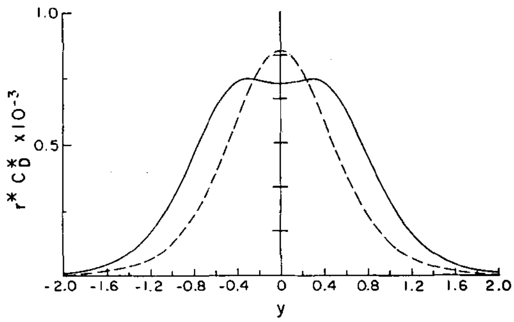

Fig. 6. Dimensionless coefficient $r^*C_D^*$ as a function of the cross-stream coordinate y. The solid curve corresponds to values for $\bar{u} = \operatorname{sech} y$, the dashed curve corresponds to $\bar{u} = 1$.

$1 + (1 + \alpha^2)^{\frac{1}{2}} \geq 2$ in (21). This difference in the magnitudes of the vertical wave numbers is solely responsible for producing a larger value of $u(x, 0, 0)$ when the basic flow is constant. Another property of the drag due to this difference in the vertical wave numbers will be pointed out in section 5.

Away from the central axis, $y = 0$, u and w differ in each case. The vertical velocity is actually smaller when $\bar{u} = \bar{u}(y)$, as is apparent from (5). In this latter case u, represented by (A1), is determined from the momentum equation

$$\bar{u}\partial u/\partial x = -v d\bar{u}/dy - \partial\pi/\partial x$$

The term $vd\bar{u}/dy$, which vanishes at $y = 0$, combines with the pressure gradient term to increase the magnitude of the u-component, such that the wave drag ultimately becomes larger at a distance corresponding to about the half-width of the hill.

The relative effect of lateral shear on the magnitude of the wave-drag is also displayed in the total drag coefficient

$$C_D = \int_{-\infty}^{\infty} C_D^*(y^*)\, dy^* \tag{29}$$

which is a nondimensional quantity. For comparison C_D was also computed for two-dimensional constant flow over the ridge $h(x, 0)$, defined by (22). The value is determined from (28) with A^* replaced by $2r^*$, the "effective area" per unit width. The evaluation is carried out in the Appendix. The various drag coefficients are:

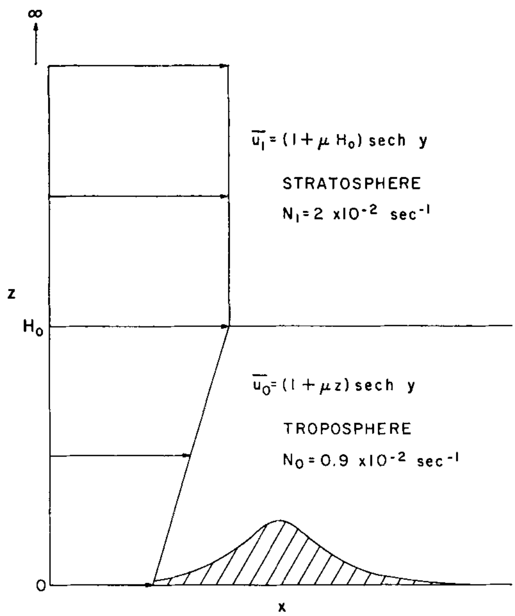

Fig. 7. Schematic representation of the two-layer model. For $H_0 = 1$ (8 km) and $\mu = 0.75$, $|\bar{u}_0^*| = 23$ m sec^{-1} and $|\bar{u}_1^*| = 40$ m sec^{-1}. The values of the Brunt-Väisälä frequency N (sec^{-1}) are indicated for each layer.

$C_D = 0.21 \times 10^{-2}$; two-dimensions, $\bar{u} = 1$

$C_D = 0.14 \times 10^{-2}$; three-dimensions, $\bar{u} = \text{sech}\, y$

$C_D = 0.11 \times 10^{-2}$; three-dimensions, $\bar{u} = 1$

The two-dimensional drag coefficient is larger in magnitude than the other values, as could be anticipated from the above discussion. The extra degree of freedom in the constant wind case reduces C_D by a factor of 2, but only a one-third reduction occurs when lateral shear is taken into account.

Finally, the surface stress may be determined from $\tau \sim \bar{\varrho} C_D U^2$. A value of order 10 dynes cm^{-2} is determined for a series of ridges situated 25 km apart, which is in agreement with previous estimates stated in the Introduction. As noted, consideration of three-dimensionality and lateral shear will reduce this value. Significant reduction will also occur if the total drag is averaged over a larger surface area.

5. Two-layer atmosphere

The sensitivity of the drag to vertical atmospheric structure, as well as to the features previously considered, will be evaluated by means of the model presented in Fig. 7. In the troposphere, the value of J, defined by (8), is $J_0 = 10$; in the stratosphere $J_1 = 16$. This structure is responsible for *partial* trapping of wave energy: resonance waves do not occur. Moreover, the value of $J_0 \gg 1/4$ is sufficiently large to prevent the occurrence of instability due to the presence of vertical shear.

In the lower layer, the basic flow (9) is

$$\bar{u}_0 = (1 + \mu z)\, \text{sech}\, y \tag{30}$$

where μ is a constant set equal to 0.75 for the present computations. The vertical structure equation for the pressure amplitude (11) reduces to

$$\xi^2 P_0'' + (m_0/\mu)^2 P_0 = 0 \tag{31}$$

where $\xi \equiv 1 + \mu z$, differentiation is with respect to ξ and m_0 is the vertical wave number given by (21). The solution may be written as the sum of an incident and a reflected wave

$$P_0 = A\xi^{1/2}[e^{ib \ln \xi} + \text{R}e^{-ib \ln \xi}] \tag{32}$$

where

$$b^2 = (m_0/\mu)^2 - 1/4 \tag{33}$$

and the two arbitrary constants of integration are given in terms of A and the reflection coefficient R. This coefficient may be expressed as

$$R = |R| e^{i\theta} \tag{34}$$

where θ represents the change of phase of the reflected wave. In the upper layer, $G = 1 + \mu H_0$ and the wave solution that satisfies (6) is

$$P_1 = Be^{im_1 z} \tag{35}$$

where

$$m_1^2 = \frac{J_1(\lambda/\alpha)^2}{(1 + \mu H_0)^2} \tag{36}$$

λ is given by (17), B is a constant and H_0 is the interface height.

The conditions that determine the arbitrary constants are (5) and the continuity of pressure and vertical velocity at the interface. The latter two conditions are expressed as

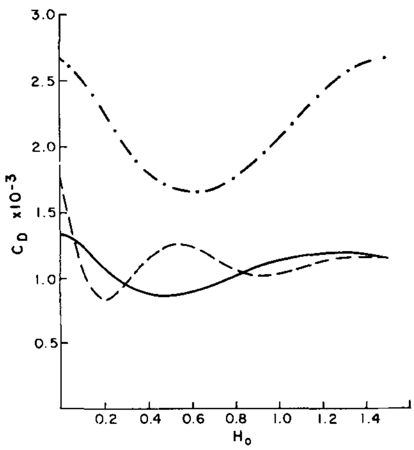

Fig. 8. Dimensionless drag coefficient C_D, given by (29), as a function of the height H_0. The curves correspond to: case 1: two-dimensions (·—·); case 2: three-dimensions and horizontal shear (– – –); case 3: three-dimensions and no horizontal shear (——). In all cases the basic flow varies in the vertical as in Fig. 7.

$$\left.\begin{aligned} P_0 &= P_1 \\ W_0 &= W_1 \end{aligned}\right\} z = H_0 \tag{37}$$

where the vertical velocity amplitude is determined from use of (18) in each layer.

The evaluation of the constants is extensive and will not be presented. The momentum flux integrals, used in the evaluation of the drag coefficient (29) are displayed in the Appendix. The drag coefficient C_D as a function of the interface height H_0, for three cases, is displayed in Fig. 8. The value at $H_0 = 0$ provides a check on the computations: C_D reduces to the drag on a one-layer atmosphere, characterized by $J_1 = 16$. If the values of C_D on the ordinate are multiplied by $(J_0/J_1)^{\frac{1}{2}} = 0.791$, agreement with the values presented in section 4 is attained. The most significant feature of the present results is the marked dependence of C_D on the interface height, although in practice $H_0 \sim 1$. This feature of the drag was noted by Blumen (1965), in association with a two-layer nonhydrostatic model. Relative maxima of the drag occur when the denominators of the integrands in the Appendix (part B) are relative minima. The maxima occur in (B 2), for example, when

$$(m_0/\mu) \ln (1 + \mu H_0) = n\pi \tag{38}$$

When the shear is weak $\mu < 1$, (38) reduces to

$$m_0 H_0 \approx n\pi \tag{39}$$

The maxima in this latter case, occur when H_0 is a multiple of one-half the vertical wavelength $L_z = 2\pi/m_0$. This condition was derived by Blumen (1965) and later extended by Klemp & Lilly (1975) to multi-layer models of surface wind speed maxima. In fact, the physical explanations for the existence of both drag and wind speed maxima are identical.

The explanation is revealed by the reflection coefficient (34), which is derived from (37) with the aid of (32), (35) and (19). We obtain

$$|R| = (J_1^{1/2} - J_0^{1/2})/(J_1^{1/2} + J_0^{1/2}) \tag{40}$$

and, neglecting small terms of order 10^{-1},

$$\begin{aligned} \theta &\approx 2b \ln (1 + \mu H_0) \\ &\approx 2(m_0/\mu) \ln (1 + \mu H_0) \end{aligned} \tag{41}$$

Note that partial reflection occurs at the interface, $0 < |R| < 1$, when $J_0 \neq J_1$, and $J_1 \neq \infty$.

In view of the basic shear flow in the lower layer, the energy flux $\overline{\pi w}$ is a function of height. The vertical momentum flux is independent of height but depends on the phase θ. According to (38) and (41), the maximum wave drag occurs when $\theta = 2n\pi$, which corresponds to maxima in the wave amplitude at ground level. When $\theta \neq 2n\pi$, interference occurs and the drag is reduced. Klemp & Lilly have generalized these results to multi-layers in order to determine the optimum conditions for surface wind enhancement.

Further information about the response can be gained from the expressions for the vertical wave numbers, l_0, m_0, and n_0, that correspond to the three cases displayed in Fig. 8. For each case we have

1) $b^2 \approx J_0/\mu^2 = l_0^2/\mu^2$

2) $b^2 \approx (J_0/\mu^2\alpha^2)[\alpha^2 + 1 + (1 + \alpha^2)^{\frac{1}{2}}] = m_0^2/\mu^2$

3) $b^2 \approx (J_0/\mu^2\alpha^2)[\alpha^2 + \beta^2] = n_0^2/\mu^2$

In the two-dimensional case l_0 is independent of wavenumber α. Consequently, C_D depends harmonically on $\ln (1 + \mu H_0)$, reaching the same amplitude in each cycle. Since the shape of C_D for case 3 is similar to that of case 1,

$$n_0^2 = J_0 \frac{\alpha^2+\beta^2}{\alpha^2} \sim l_0^2$$

where $\beta^2 < \alpha^2$. However, in case 2

$$m_0^2 = J_0 \frac{\alpha^2 + [1+(1+\alpha^2)^{1/2}]}{\alpha^2}$$

The counterpart of β^2 in the above is $1 + (1+\alpha^2)^{\frac{1}{2}} \geqslant 2$. Horizontal shear, in this case, reduces the vertical wavelength to the extent that two maxima of C_D occur over one cycle of each of the other two cases.

The sensitivity of the drag to the presence of horizontal shear flow should also be evident in a more realistic atmospheric model, since the physical effect that produces the characteristic response has been shown by Klemp & Lilly to be enhanced, for example, in a three-layer model.

6. Remarks

The principal results of the present study are associated with the presence of cross-stream shear of the basic flow. Two significant features, affecting the wave drag by stationary mountain lee-waves, are noted: since the basic flow is assumed to vanish at large cross-wind distances from the mountain, the wave disturbance is primarily restricted to a channel essentially bounded by the characteristic diameter of the hill (see Fig. 4). An effect of this concentration is the maintenance of a relatively large drag coefficient as exemplified in Fig. 6. Partial reflection at the tropopause, in a two-layer representation of the atmosphere, affects the magnitude of the drag because this latter quantity is sensitive to the phase difference between the incident and reflected waves. This phase difference is shown to be directly related to the ratio of the vertical wavelength of the disturbance to the layer depth H_0, which is significantly affected by the presence of cross-stream shear.

The present results have not been subjected to direct observational verification, but evidence presented by Klemp & Lilly (1975) shows that linear lee-wave theory is capable of capturing the essence of the atmospheric response to partial reflection in a stably stratified atmosphere. Their results were obtained for hydrostatic flow over a ridge, so that three-dimensional effects were omitted. However, they showed that the neglect of nonhydrostatic effects, for long waves, could be supported by comparing their model predictions with observations.

It is very difficult to justify the neglect of nonlinearity, together with the possibility of upstream blocking, rotors and flow around an isolated hill, particularly in the explicit evaluation of the drag exerted on the atmosphere. We have also pointed out (in section 2), that the steady-state assumption is strictly indefensible, particularly when inertial instabilities are present. However, the steady-state assumption has been frequently employed, with an indication that some observational aspects of lee-waves have been well-modelled. In conclusion, we feel that the present model does capture the essence of cross-stream shear on lee-waves and that these effects should be kept in view when parameterization of subgrid-scale processes are undertaken.

Acknowledgements

This investigation was supported by the Atmospheric Science Section of the National Science Foundation, under Grant GA-31868. We are grateful to J. Klemp and R. Smith, whose comments have been very helpful in the preparation of the manuscript.

Appendix. Momentum flux integrals

A. *One-layer atmosphere*

The horizontal velocity components (u, v) for the case when $\bar{u} = \operatorname{sech} y$ are given by

$$u(x,y,z) = -\operatorname{Re} i \int_0^\infty \left\{ \frac{J_0}{\alpha^2 m} \gamma(\gamma-1) + \left(m - \frac{J_0 \gamma_2}{\alpha^2 m}\right) \operatorname{sech}^2 y \right\} (1+\alpha^2)^{-1/2} \times \exp[-(\eta + \ln \cosh y)(1+\alpha^2)^{1/2} + i(\alpha x + mz)]\, d\alpha \quad \text{(A 1)}$$

and

$$v(x, y, z) = \mathrm{Re} \tanh y J_0 \int_0^\infty \frac{\gamma}{\alpha m} (1+\alpha^2)^{-1/2} \times \exp[-(\eta + \ln \cosh y)(1+\alpha^2)^{1/2} + i(\alpha x + mz)] d\alpha, \quad (A\,2)$$

where J_0, γ and m are given by (8), (16) and (21). As a check, (23), (A 1) and (A 2) satisfy the continuity equation for this Boussinesq model,

$$u_x + v_y + w_z = 0$$

The integral in (28) is evaluated by interchanging the order of integration and making use of the expression

$$2\pi\delta(\alpha - \alpha') = \int_{-\infty}^{\infty} e^{i(\alpha-\alpha')x} dx \quad (A\,3)$$

where $\delta(\alpha - \alpha')$ is the Dirac delta-function, which has the property that

$$\int_0^\infty \delta(\alpha - \alpha') f(\alpha, \alpha') d\alpha' = f(\alpha) \quad (A\,4)$$

and f is a function of the indicated variables. The evaluation yields

$$-\int_{-\infty}^{\infty} uw\,dx = \pi J_0^{1/2} \operatorname{sech}^2 y \int_0^\infty (1+\alpha^2)^{-5/4} \times \exp[-2(\eta + \ln\cosh y)(1+\alpha^2)^{1/2}] \times [1 + (1+\alpha^2)^{1/2}]^{1/2}[[1+\alpha^2)^{1/2} - \operatorname{sech}^2 y] d\alpha \quad (A\,5)$$

This expression (A 5) for the momentum flux integral is independent of height z as expected from the extension to three-dimensions of the theorem derived by Eliassen & Palm (1960). Moreover, there is no contribution to the stress from $v(x, y, z)$ because this component is 90 degrees out of phase with both u and w.

A similar computation may be carried out for the three-dimensional case corresponding to $\bar{u} = 1$. The details are omitted, but the final result is

$$-\int_{-\infty}^{\infty} uw\,dx = \pi J_0^{1/2} \operatorname{sech} y \times \int_{-\infty}^{\infty}\int_0^\infty \alpha^2(\alpha^2+\beta^2)^{-1/2}(1+\alpha^2)^{-1} \times \exp[-(2\eta + \ln\cosh y)(1+\alpha^2)^{1/2}] \times F(\alpha, \beta) \cos \beta y\, d\alpha\, d\beta \quad (A\,6)$$

where $F(\alpha, \beta)$ is given by (26).

Similarly, the two-dimensional case, for $\bar{u} = 1$, reduces to

$$-\int_{-\infty}^{\infty} uw\,dx = \pi J_0^{1/2} \int_0^\infty \alpha(1+\alpha^2)^{-1} \times \exp[-2\eta(1+\alpha^2)^{1/2}] d\alpha \quad (A\,7)$$

If the variable

$$\zeta = (1+\alpha^2)^{\frac{1}{2}} - 1$$

is introduced into (A 7), we obtain

$$-\int_{-\infty}^{\infty} uw\,dx = \pi J_0^{1/2} \int_0^\infty (1+\zeta) \exp[-2\eta(1+\zeta)] d\zeta = \pi J_0^{1/2} E_1(2\eta) \quad (A\,8)$$

where $E_1(2\eta)$ denotes the Exponential Integral which may be evaluated from tables presented by Gautschi & Cahill (1964).

B. *Two-layer atmosphere*

The integrands of (A 5), (A 6) and (A 7) will be denoted respectively by f_5, f_6, and f_7. Then the momentum flux integrals are given by the following expressions:

two-dimensions $[\bar{u} = (1 + \mu z)]$

$$-\int_{-\infty}^{\infty} uw\,dx \approx \pi J_1^{1/2} \times \int_0^\infty \frac{f_7}{1 + \left(\frac{J_1}{J_0} - 1\right) \sin^2\left(l_0 \frac{\ln(1+\mu H_0)}{\mu}\right)} d\alpha \quad (B\,1)$$

three-dimensions $[\bar{u} = (1 + \mu z) \operatorname{sech} y]$

$$-\int_{-\infty}^{\infty} uw\,dx \approx \pi J_1^{1/2} \operatorname{sech}^2 y \times \int_0^\infty \frac{f_5}{1 + \left(\frac{J_1}{J_0} - 1\right) \sin^2\left(m_0 \frac{\ln(1+\mu H_0)}{\mu}\right)} d\alpha \quad (B\,2)$$

three-dimensions $[\bar{u} = (1 + \mu z)]$

$$-\int_{-\infty}^{\infty} uw\,dx \approx \pi J_1 \operatorname{sech} y$$

$$\times \int_{-\infty}^{\infty}\int_{0}^{\infty} \frac{f_6}{1+\left(\dfrac{J_1}{J_0}-1\right)\sin^2\left(n_0\dfrac{\ln(1+\mu H_0)}{\mu}\right)} \times d\alpha\, d\beta \qquad (B\,3)$$

where the vertical wavenumbers (l_0, m_0, n_0) are given by 1), 2) and 3) on p. 295. The above expressions have been simplified by omitting terms less than order

$$\frac{\mu}{2J_0^{1/2}} \sim 10^{-1}.$$

The drag coefficient C_D is determined from (28) and (29), using the appropriate integral above.

REFERENCES

Blumen, W. 1965. A random model of momentum flux by mountain waves. *Geofys. Publ. 26*, 1–33.

Blumen, W. 1971*a*. Hydrostatic neutral waves in a parallel shear flow of a stratified fluid. *J. Atmos. Sci. 28*, 340–344.

Blumen, W. 1971*b*. Jet flow instability of an inviscid compressible fluid. *J. Fluid Mech. 46*, 737–747.

Blumen, W. 1975. Stability of non-planar shear flow of a stratified flow. *J. Fluid Mech. 68*, 177–189.

Bretherton, F. P. 1969. Momentum transport by gravity waves. *Quart. J. R. Met. Soc. 95*, 213–243.

Eliassen, A. & Palm, E. 1961. On the transfer of energy in stationary mountain waves. *Geofys. Publ. 22*, 1–23.

Erdélyi, A., Magnus, W., Oberhettinger, F. & Tricomi, F. G. 1954. *Tables of Integral Transforms*, vol. 1. Bateman Manuscript Project. McGraw-Hill, New York, 391 pp.

Foldvik, A. & Wurtele, M. G. 1967. The computation of the transient gravity wave. *Geophys. J. R. Astr. Soc. 13*, 167–185.

Gautschi, W. & Cahill, W. F. 1964. Exponential integral and related functions. In *Handbook of Mathematical Functions* (ed. M. Abramowitz and I. A. Stegun), chap. 5, pp. 227–251. U.S. Government Printing Office, Washington, D.C.

Klemp, J. B. & Lilly, D. K. 1975. The dynamics of wave-induced downslope winds. *J. Atmos. Sci. 32*, 320–339.

Lilly, D. K. 1972. Wave momentum flux—a GARP problem. *Bull. Amer. Meteor. Soc. 53*, 17–23.

Queney, P. 1948. The problem of air flow over mountains: A summary of theoretical studies. *Bull. Amer. Meteor. Soc. 29*, 16–26.

Sawyer, J. S. 1959. The introduction of the effects of topography into methods of numerical forecasting. *Quart. J. R. Met. Soc. 85*, 31–43.

Smith, R. B. 1976. The generation of lee waves by the Blue Ridge. *J. Atmos. Sci. 33*. 507–519.

Wurtele, M. G. 1957. The three-dimensional lee wave. *Beitr. Phys. frei Atmos. 29*, 242–252.

ВОЛНОВОЕ СОПРОТИВЛЕНИЕ ТРЕХМЕРНЫХ ВОЛН ЗА ГОРАМИ В НЕПЛОСКОМ ПОТОКЕ С ВЕРТИКАЛЬНЫМ СДВИГОМ СКОРОСТИ

В линейном гидродинамическом приближении рассматривается влияние как поперечного, так и вертикального градиента скорости основного потока на стационарные волны за горами в устойчиво стратифицированном потоке воздуха. Сначала при постоянном градиенте температуры для основного состояния находятся аналитические решения. Решение, соответствующее изменению ветра в поперечном направлении, описываемому профилем в виде гиперболического секанса, сравнивается с решением, соответствующим постоянному потоку над той же изолированной горой. В первом случае энергия волн захватывается полем окружающего сдвига ветра. Этот эффект ответствен за большее волновое сопротивление потоку, чем в случае постоянного ветра. Однако эти величины волнового сопротивления всегда меньше, чем сопротивление, оказываемое двумерными волнами за хребтом. Затем рассматривается двухслойная модель с целью изучения влияния устойчивой стратосферы над менее устойчивой тропосферой. Результаты указывают на то, что на сопротивление влияет разность фаз между излучаемой и отраженной волнами в нижнем слое. Это влияние более выражено, если учитывается поперечный градиент скорости основного потока. Наконец, указывается на связь между динамикой в данной модели и механизмон Клемпа и Лилли, предложенным для динамики ветров в направлении вниз по склону, возбуждаемых волнами.